Caisson Foundations Subjected to Reverse Fault Rupture: Centrifuge Testing and Numerical Analysis

M. Loli[1]; I. Anastasopoulos[2]; M. F. Bransby[3]; W. Ahmed[4]; and G. Gazetas, M.ASCE[5]

Abstract: Recent large-magnitude ($M > 7$) earthquakes have caused numerous failures induced by surface faulting, demonstrating the need to account for tectonic deformation in seismic design. Thanks to their usually high rigidity, embedded (e.g., caisson) foundations may divert the fault rupture and lead to favorable performance, whereas surface or piled foundations may fail. We present a series of centrifuge model tests to investigate the response of caisson foundations embedded in a cohesionless soil stratum, the base of which is subjected to reverse faulting. We elucidate the interplay between the propagating fault rupture and the caisson, focusing on the role of the location of the outcropping rupture relative to the caisson. The rigid-body of the caisson causes diversion and/or bifurcation of the shear localization, which is forced to develop preferentially around the edges of the caisson. The observed failure pattern and the consequent caisson response depend strongly on the exact caisson position relative to the fault. We employed three-dimensional (3D) finite-element (FE) modeling and validated it by comparing to centrifuge test results. The numerical method captures the general interaction mechanisms, showing satisfactory (if not always perfect) agreement with experiments. We then employ the validated numerical method in a parametric investigation, providing further insight into the different possible modes of foundation response. **DOI: 10.1061/(ASCE)GT.1943-5606.0000512.** © *2011 American Society of Civil Engineers.*

CE Database subject headings: Finite element method; Three-dimensional models; Caissons; Numerical analysis; Earthquakes; Geological faults.

Author keywords: Thrust fault; Finite elements; 3D analysis; Caisson foundations; Centrifuge modeling; Soil-caisson-rupture interaction; Tectonic deformation.

Introduction

Earthquakes are generated on faults in the Earth's crust and are categorized according to the relative movement between displaced blocks: strike-slip faults (horizontal shearing and relative movement along the strike) and dip-slip faults (vertical shearing and relative movement along the dip). The latter are further classified into reverse (or thrust) type, in which upward movement of the hanging wall prevails or a net compression of the soil layer occurs, and normal, in which the opposite occurs.

Such subterranean movements usually affect surface engineered facilities only indirectly, through emitted waves and the resulting ground shaking. In large-magnitude earthquakes, the causative fault may propagate all the way to the ground surface and outcrop (see, for example, Sherard et al. 1974), significantly deforming any overlying structure along the rupturing path. A number of recent seismic events (Kocaeli, Turkey, in 1999; Düzce, Turkey, in 1999; Chi-chi, Taiwan, in 1999; and Wenchuan, China, in 2008) have been characterized by extensive damage to structures because the fault rupture emerged directly beneath them. These events highlight the need to account for tectonic loading in seismic design.

The 1999 Chi-chi earthquake in Taiwan offered probably the most spectacular demonstration of the fault rupture hazard. Extending over a distance of nearly 90 km and reaching an extreme vertical offset of 10 m, the thrust surface rupture caused a great variety of structural failures that have been well documented (Chang et al. 2000; Kelson et al. 2001a, b; Kawashima 2001; Dong et al. 2004; Angelier et al. 2003; Faccioli et al. 2008).

More recently, in May 2008, the Wenchuan earthquake struck the western central part of China, resulting in the longest surface fault rupture documented to date. Tectonic deformation occurred simultaneously along three major preexisting faults that cross the Longmen Shan thrust belt at the eastern margin of the Tibetan plateau, resulting in an approximately 285-km-long surface rupture zone (Lin et al. 2009; Xu et al. 2009; Jia et al. 2009). Two major fault scarps (260 km along the Yingxiu-Beichuan thrust fault and 70 km along the Pengguan thrust fault) developed within a relatively narrow surface soil band measuring less than 10 km wide, producing up to a 6.5-m permanent vertical ground displacement. The surface reverse fault ruptures crossed several urban areas, affecting a large number of buildings, lifelines, and transportation facilities. Fig. 1 presents a selection of images, showing examples of such fault rupture–structure interaction events.

The eyecatching faulting-induced failures occurring in these earthquakes attracted the attention of several researchers and gave rise to the question: Is it feasible to design structures to withstand surface fault emergence?

[1]Graduate Student, Univ. of Dundee, Nethergate, Dundee, DD1 4HN, U.K. E-mail: mariannaloli@yahoo.com

[2]Adjunct Lecturer, National Technical Univ. of Athens, Heroon Polytechniou 9, 15780, Zografou, Greece. E-mail: ianast@civil.ntua.gr

[3]Senior Lecturer, Univ. of Dundee, Nethergate, Dundee, DD1 4HN, U.K. E-mail: m.f.bransby@dundee.ac.uk

[4]Graduate Student, Univ. of Dundee, Nethergate, Dundee, DD1 4HN, U.K. E-mail: w.ahmed@dundee.ac.uk

[5]Professor, National Technical Univ. of Athens, Heroon Polytechniou 9, 15780, Zografou, Greece (corresponding author). E-mail: gazetas@ath.forthnet.gr

Note. This manuscript was submitted on December 28, 2009; approved on January 20, 2011; published online on January 22, 2011. Discussion period open until March 1, 2012; separate discussions must be submitted for individual papers. This paper is part of the ***Journal of Geotechnical and Geoenvironmental Engineering***, Vol. 137, No. 10, October 1, 2011. ©ASCE, ISSN 1090-0241/2011/10-914–925/$25.00.

Fig. 1. Examples of reverse fault rupture interaction with structures during the 2008 Wenchuan earthquake in China: (a) the school building on the left was driven 2 m upward, standing on the "moving wall," and survived the fault-induced deformation practically unscathed; (b) front view of the school building; (c) failure of a three-story building, which was crossed by a fault rupture of 1 m throw; (d) collapse of a bridge span from fault-induced differential displacement of its piers (reprinted with permission from Lin and Ren 2009)

In response to this question, several studies have considered the response of a structural system interacting with a propagating fault rupture, revealing that the presence of a structure may alter—sometimes dramatically—the free-field rupture path. The mechanics of this phenomenon, termed fault rupture–soil–foundation–structure interaction (FR-SFSI), have been analyzed on the basis of interpretation of real case histories (Anastasopoulos and Gazetas 2007a), centrifuge experiments (Bransby et al. 2008a, b; Ahmed and Bransby 2009), and numerical analyses (Gazetas et al. 2007; Yilmaz and Paolucci 2007; Paolucci and Yilmaz 2008; Anastasopoulos et al. 2008, 2009). One of the most significant conclusions was that the foundation, depending on its rigidity and continuity, may play the most important role in the system's response, with its ability to cause partial or even complete diversion of the rupture and thereby control the survival of the structure under the imposed loading. Compiling current research findings, Gazetas et al. (2008) attempted a preliminary answer to the question of designing structures to withstand surface fault emergence, highlighting the crucial role of the foundation system in fault-tolerant design.

In this paper, we aim to extend the research work on the mechanisms of FR-SFSI, which is currently more or less limited to the response of shallow foundations. We investigate the interaction of deep embedded foundations (i.e., caissons) with a rupturing reverse fault, and we assesses their seismic design for faulting conditions.

Fault Rupture–Caisson Foundation Interaction: Problem Definition

When a reverse fault ruptures in the free field (i.e., in the absence of a foundation), deformation localizes along a single rupture plane. In particular, reverse faults are generally expected to decrease in dip while propagating toward the ground surface, with the hanging wall bending over the footwall (Cole and Lade 1984; Bray et al. 1994b). However, it has been observed that the rupture pattern differs when a foundation interacts with the free-field rupture plane, as observed, for example, for surface foundations in Kelson et al. (2001) and Anastasopoulos and Gazetas (2007b).

Depending on the relative to the fault position, the geometry, and the surcharge load, shallow foundations may cause total diversion or only partial diversion of the fault rupture (Ahmed and Bransby 2009; Anastasopoulos et al. 2008, 2010). In the latter case, the distress of the structural system is primarily caused by the loss of support under the edges or around the center of the foundation base and by its rigid-body displacement. The response is thought to be quite different when a propagating fault interacts with a much stiffer caisson foundation. Intuitively, we would anticipate that introducing a rigid caisson in the path of the free-field rupture acts as a kinematic constraint, which impedes the propagation of tectonic deformation, forcing the rupture to deviate and develop outside the foundation margins. This idea is supported by a number of field observations on the effect of massive, rigid structures on the surface propagation of fault scarps. For example, Kelson et al. (2001a, b) document that the surface scarp of the Chelungpu fault during the 1999 Chi-chi earthquake appeared in several cases to change strike direction, avoiding buildings with massive foundations.

Fig. 2 shows the only case history known to the authors of a reverse fault interacting with a single caisson foundation. The illustrated electricity pylon, located at Min-Chien City, Taiwan, was crossed by the Chelungpu fault, and was subjected to a relative displacement of approximately 4 m. Fig. 2(a) displays our interpretation of the fault-caisson interaction mechanism taking place in

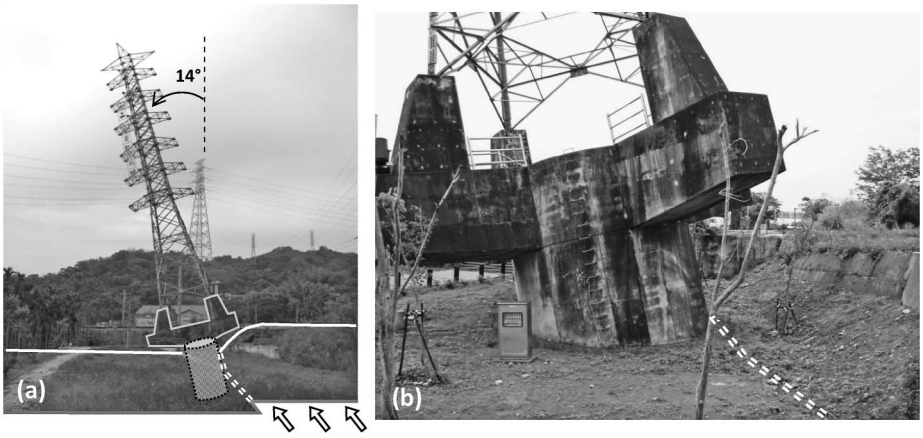

Fig. 2. A case history of reverse fault rupture interaction with a caisson foundation: (a) a high-voltage electricity pylon supported on a rigid caisson was crossed by the Chelungpu fault during the 1999 Chi-chi earthquake in Taiwan; (b) closer view of the circular (5 m in diameter) caisson, showing the soil surface bulging on its right side because of the fault outcrop (photographs by Marianna Loli)

this case. It is likely that the fault rupture, interacting with the 5-m-diameter rigid caisson, diverted toward the hanging wall [as shown in Fig. 2(a)]; hence, a soil bulge formed beside the caisson because of the fault emerging on the surface [Fig. 2(b)]. Interestingly, although this caisson caused diversion of the fault and the pylon remained at the stationary side of the ground (i.e., on the footwall), the pylon experienced a surprisingly large rigid-body rotation of 14°. Yet in contrast to what was the case for other structures in the same area (where different foundation types had been used), no evident structural damage appears to have occurred in the pylon. This may be the first evidence of the advantageous performance of caisson foundations when subjected to faulting.

This paper investigates the qualitatively similar fault-caisson interaction problem, which is illustrated schematically in Fig. 3. In particular, a rigid (typical for medium-span bridges; see Anastasopoulos et al. 2009) A $B \times B \times D$ caisson foundation is considered, in which $B = 5$ m (breadth and length) and $D = 10$ m (embedment depth), supported on a 15-m-thick layer of dense ($D_r \approx 80\%$) dry sand. The caisson carries a total vertical load of approximately 20 meganewtons (MN), which represents the weight of a superstructure of significant size (for example, a medium-span bridge). Thrust fault displacement of vertical amplitude h (throw) is applied at bedrock. The displaced block (the hanging wall) moves upward with a dip angle of 60°, whereas the footwall remains stationary. The fault deformation forces the caisson to move as a rigid body, experiencing both translational and rotational displacements.

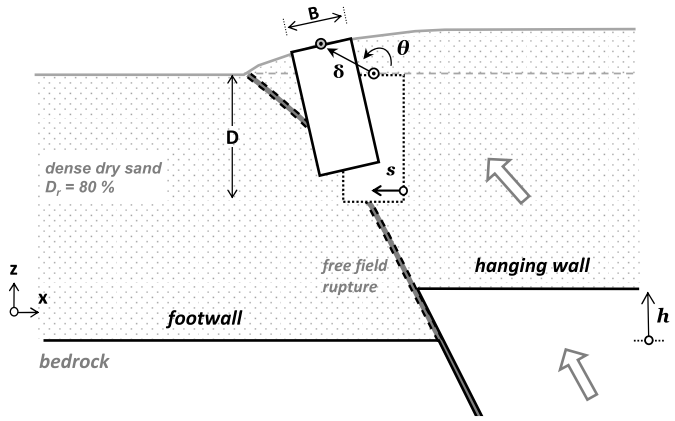

Fig. 3. Schematic illustration of the studied problem

The caisson movement will be quantified by the rotation θ and the displacement vector δ (δ_x and δ_z, referring to horizontal and vertical component, respectively), measured at the caisson top side middle point (the base of the supported bridge pier), so as to be representative of the tectonic deformation transmitted onto the superstructure (Fig. 3).

We used a combination of experimental and numerical work to strengthen the validity of the derived conclusions. More specifically, we reported the results from a series of centrifuge model tests investigating fault rupture propagation in the free field and its interaction with a caisson foundation, with emphasis on the effect of foundation position. We then employed nonlinear 3D finite-element (FE) simulation of the problem and validated through comparison with experimental results. Finally, we used the validated FE method to carry out a thorough parametric study on the effect of the exact caisson position relative to the fault. We identified different interaction mechanisms taking place for different caisson positions, and we discuss the consequent system response.

Centrifuge Modeling

We conducted a series of centrifuge model tests in the beam centrifuge of the University of Dundee, U.K., at an operational acceleration of 100 g. Hence, we applied a scale factor of $N = 100$ to all dimensions of the prototype problem (e.g., Schofield 1980). The experimental study aimed at investigating the fault mechanisms taking place at different positions of the caisson. This is expressed by parameter s, which is defined as the distance between the caisson right corner and the point that the free-field fault rupture would cross the foundation base (Fig. 3). In other words, s indicates the point that the fault rupture would "meet" the caisson if interaction did not occur to alter the rupture path.

We report three centrifuge tests: Tests ML-03, ML-04, and ML-05. In each case, the caisson was placed at a different position. We also include one test without a foundation, Test WA-01, to provide the free-field reference.

Model Preparation

A photograph of the centrifuge model inside the strongbox is shown in Fig. 4(a) as it was deformed after we completed Test ML-05, in which the caisson was placed at a position $s/B = 0.22$. The 150-mm-deep (15–m-deep at prototype scale) soil layer was prepared by dry air pluviation of Fontainebleau sand

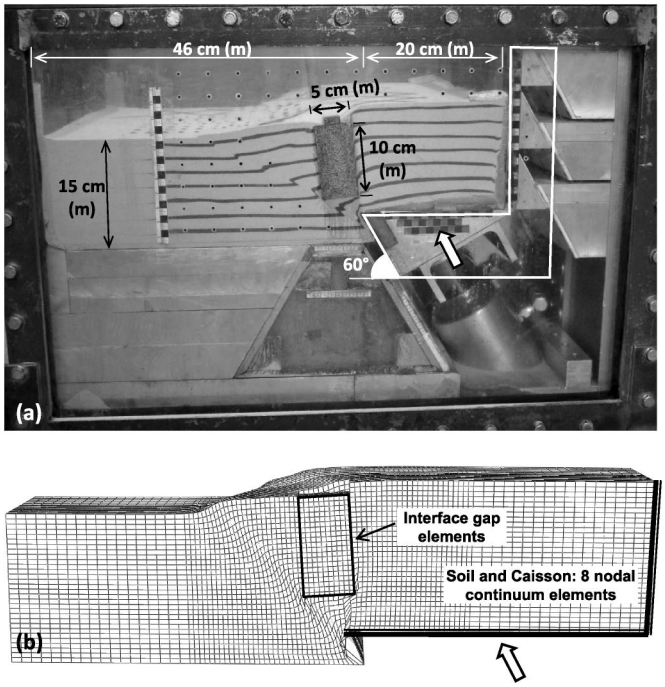

Fig. 4. Combined experimental and numerical study: (a) photo of the faulting apparatus (split box) and the centrifuge model after completion of a test (indicatively for $s/B = 0.22$), showing the main features and dimensions (units: cm for the model; m in parentheses for prototype); (b) snapshot of deformed FE mesh

(Gaudin 2002). The sand was pluviated from a specific height with a fixed sieve aperture to control the mass flow rate, giving it a uniform density $D_r \approx 80\%$ ($\gamma = 16.11$ kN/m^3).

We conducted direct-shear tests to investigate the soil stress-strain and volumetric behavior. For a mean value of relative soil density $D_r = 80\%$, the peak and residual friction angles of the soil measured $\varphi_{peak} = 37°$ and $\varphi_{res} = 31°$ at a normal effective stress representative of the middle of the soil depth (i.e., $\sigma'_v = 120$ kPa (kilopascals) for depth $z = -7.5$ m). We measured the dilation angle ψ, which depends significantly on the effective stress (Bolton 1986), as approximately 10° for the same representative normal stress.

The model caisson was made of steel, with a total mass of 1.025 kg [corresponding to a prototype of 2,050 megagrams (Mg)]. Aiming to have realistically rough soil-caisson interfaces, we needle-gunned the model caisson sides (except the side facing the Perspex window of the strongbox). We measured the frictional properties at the caisson-soil interface through direct-shear tests performed on similar needle-gunned steel specimens, which gave a friction angle of 19.8° at peak and 17° at residual conditions.

We determined the horizontal caisson position (x) with regard to the free-field rupture trace so that the free-field rupture would cross the caisson body at a distance s from its right base corner (Fig. 3). We placed the model caisson against the Perspex, which we assumed to act as a plane of symmetry. Hence, the model dimensions perpendicular to this plane were one-half of the originally considered (prototype) values.

Instrumentation

The apparatus used for this study, shown in Fig. 4(a), has been used in the past in a variety of similar faulting problems and has been described in detail in El Nahas et al. (2006) and Bransby et al. (2008a). We used a split box of dimensions $655.9 \times 500 \times 220$ mm to apply fault deformation at the base of the model (bedrock). We used a hydraulic actuator to make the moving part of the box translate upward during spinning in a controllable quasi-static manner, reaching fault throw amplitudes of about 35 mm. The split box was constructed within a centrifuge strongbox [see Fig. 4(a)], which contained the soil-foundation model.

The strongbox has a front and back face made of Perspex to allow taking digital images of the deformed model during testing. We used a pair of digital cameras to take photos of the model side [the face observed in Fig. 4(a) and plan view—top face in Fig. 4(a)] during testing. We took approximately 100 pairs of pictures per test at progressively increasing fault offsets. We then analyzed the photographic data using the GeoPIV program (GeoPiv 2007; White et al. 2003) to calculate fault throws, caisson displacements, and the shear strains developed within the soil.

We placed a single linear variable differential transformer (LVDT) vertically on the rigid moving part of the split box to directly measure the vertical component of fault displacement (throw) during testing. We used this to monitor the progress of fault actuation during the test and to validate the results of the digital image analyses.

Numerical Simulation

We performed numerical simulations of the centrifuge model tests employing the FE method, using the ABAQUS code. Despite the unavoidable shortcoming of the FE method for modeling the localization of shear failure within a realistically thin soil band, previous studies have shown that it can simulate quite satisfactorily the phenomenon of fault rupture propagation in the free field (Roth et al. 1982; Bray et al. 1994a; Anastasopoulos et al. 2007c; Loukidis et al. 2009) and during fault-foundation interaction (Anastasopoulos et al. 2008).

Bray et al. (1994a) revealed the need to account for the nonlinear stress-strain soil behavior to effectively simulate the fault rupture propagation phenomenon, and they indicated that an adequately refined mesh is required. Following such recommendations, we performed nonlinear numerical analysis of the problem using a rather refined FE mesh. We chose the model dimensions to be the same as the dimensions of the physical model at prototype scale [Fig. 4(a)], and we set the minimum element width at the area surrounding the caisson equal to 0.5 m. We used eight-node linear strain elements and the whole mesh had 181,878 degrees of freedom (DOF). Fig. 4(b) shows the 3D deformed FE mesh for $s/B = 0.22$ for comparison to the physical model [Fig. 4(a)]. Only half of the model was simulated, taking advantage of symmetry on the vertical plane that crosses the centerline of the foundation (which corresponds to the location of the Perspex front face in the centrifuge models). Also, the geometry of the model fulfills the requirement of having an aspect ratio (length of model/depth) greater than four, as suggested by Bray et al. (1994a) to avoid boundary effects.

Soil Constitutive Modeling

We modeled soil with hexahedral continuum finite elements. We employed the elastoplastic constitutive relationship described in Anastasopoulos et al. (2007c): Mohr-Coulomb failure criterion combined with isotropic strain softening. We implemented the model in ABAQUS through a user subroutine in which the friction (φ) and dilation (ψ) angles of soil degrade linearly with the increase of octahedral plastic shear strain γ_{oct}

$$\varphi; \quad \psi = \left\{ \begin{array}{ll} \varphi_p - \frac{\varphi_p - \varphi_{\text{res}}}{\gamma_f^P} \gamma_{\text{oct}}^P; \psi_p \left(1 - \frac{\gamma_{\text{oct}}^P}{\gamma_f^P}\right), & \text{for } 0 \le \gamma_{\text{oct}}^P < \gamma_f^P \\ \varphi_{\text{res}}; \psi_{\text{res}} = 0, & \text{for } \gamma_{\text{oct}}^P \ge \gamma_f^P \end{array} \right\} \tag{1}$$

in which φ_p and ψ_p = peak mobilized friction and dilation angles, φ_{res} and $\psi_{\text{res}} = 0$ = their residual values, and γ_f^P = octahedral plastic shear strain at the end of softening. Preyield behavior was assumed to be elastic, with secant shear modulus G_S linearly increasing with depth. We accounted for scale effects from shear band thickness through an approximate simplified scaling method described by Anastasopoulos et al. (2007c). We calibrated constitutive model parameters based on the results of the direct-shear tests previously discussed.

Modeling Caisson and Soil-Caisson Interface

We modeled the body of the caisson with elastic hexahedral continuum elements that were assigned the Young's modulus and unit weight of steel. We modeled the soil-caisson interface using contact elements to allow sliding and/or detachment (loss of contact) to occur. We calibrated the interface properties to match the frictional properties of the steel-sand interface as measured in the direct-shear tests. Interested in the large strain domain, we assumed residual conditions were representative of the soil-caisson interface behavior; e.g., we set the friction angle of the interface equal to $\delta_{\text{res}} = 17°$. Since the measured difference between the peak (δ_{peak}) and residual (δ_{res}) friction angle is relatively small, we believe this simplification is reasonable.

Results for Fault Rupture in Free Field

We discuss results from the free-field test (Test WA-01) first, as a reference for the interaction tests. Fig. 5 shows the deformed soil model resulting from bedrock dislocation $h = 3.5$ m, and it compares the centrifuge experiment [Fig. 5(a)] to the numerical analysis

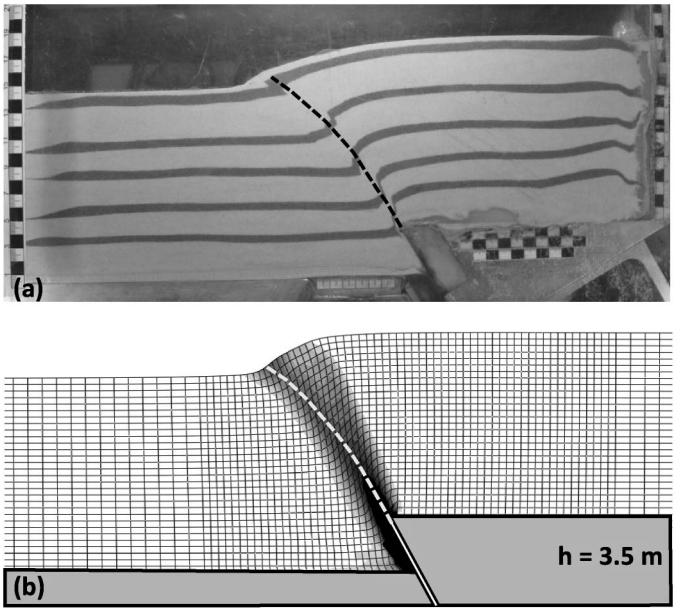

Fig. 5. Soil model deformation during fault rupture in the free field; comparison between (a) photo of the centrifuge model (Test WA-01) and (b) FE deformed mesh with superimposed plastic strains, for fault throw $h = 3.5$ m

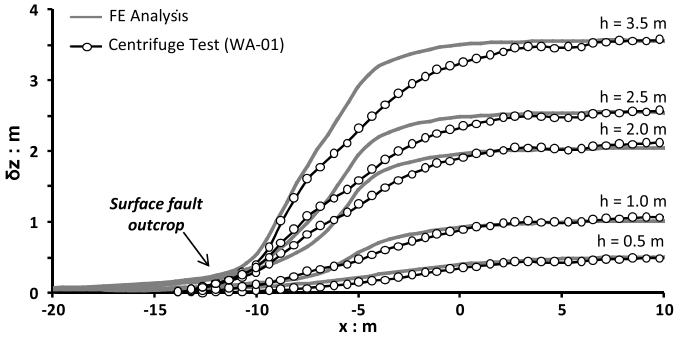

Fig. 6. Fault rupture in the free field: comparison between analysis and experiment in terms of vertical displacement profiles at the soil surface for a range of fault throw amplitudes ($h = 0.5$–3.5 m)

[Fig. 5(b)], emphasizing the shape of the failure plane. The analysis appears to agree qualitatively with the experiment, predicting well the shape of the failure surface. In addition, both the experimental and analytical fault rupture profiles agree with the previously discussed typical reverse fault rupture patterns. The rupture plane follows the bedrock dip angle (60°) for approximately the first 5 m of soil above bedrock, and then the dip decreases progressively as it propagates toward the surface.

Fig. 6 shows the vertical displacement profile at the soil surface and compares analytical prediction to experimental results, demonstrating quite satisfactory agreement for the whole range of the studied fault magnitudes ($h = 0.5$–3.5 m). The only discrepancy refers to the gradient of the surface scarp near the crest, which appears shallower in the test. Being presumably associated with the disagreement between experiment and analysis on the magnitude of shear strain, this discrepancy arises from the simplifications made during modeling of the postpeak soil behavior (note that it becomes evident for $h > 0.5$ m when the soil in the surface has entered the softening mode of response). Yet despite the limitations of the numerical methodology in accurately predicting the magnitude of shear strain, which have been comprehensively discussed in Anastasopoulos et al. (2007c), the analysis captures accurately the shape of the rupture path and provides excellent prediction of the fault outcropping location. This appears at a horizontal distance of approximately 11 m (toward the footwall) from the bedrock dislocation point. For all graphs presented hereafter, the horizontal position axis (x) is plotted such that zero represents the position of fault initiation at bedrock, with the positive sign pointing toward the hanging wall.

Results for Fault Rupture–Caisson Interaction

We discuss below the mechanisms of fault rupture–caisson interaction and the consequent response of the soil-foundation system for three different positions of the caisson relative to the fault ($s/B = -0.78$, 0.22, and 0.62).

Caisson at s/B = −0.78 with Reference to Fault (Test ML-04)

In this test, we positioned the caisson left of the fault bedrock initiation point in such a way that the free-field rupture would strike the right sidewall of the caisson approximately in the middle (i.e., the free-field fault rupture would cross the level of the caisson base $0.78B$ to the right of the caisson). Fig. 7(a) portrays the deformed centrifuge model (side and plan view) for fault throw $h = 3$ m, highlighting the observed fault rupture–caisson interaction mechanisms.

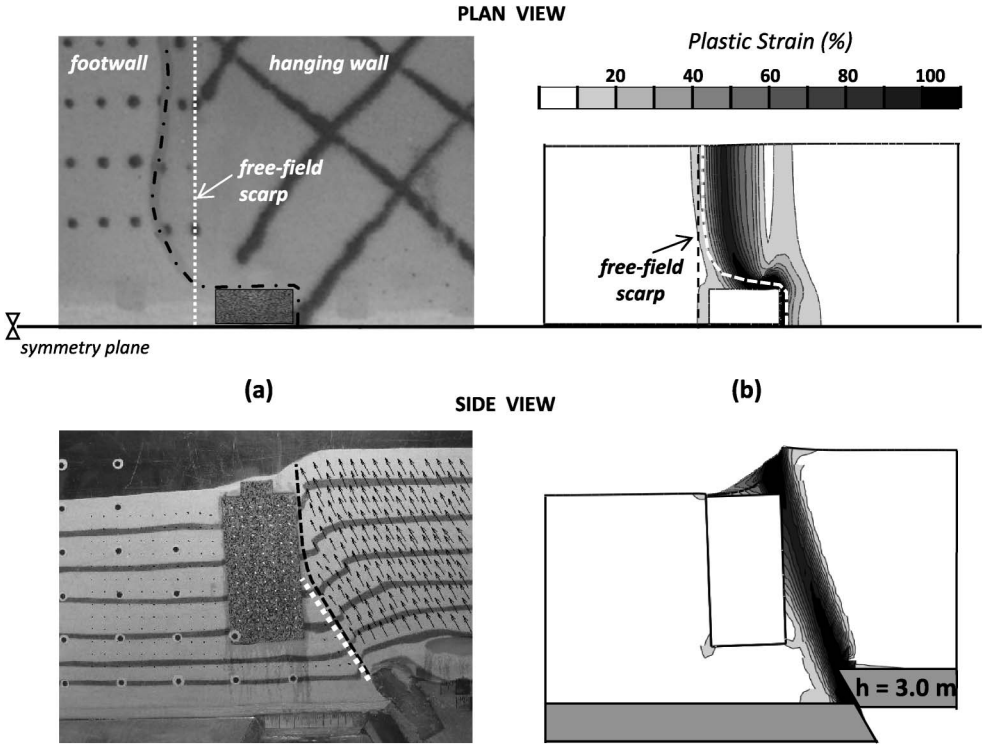

Fig. 7. Fault rupture–caisson interaction mechanisms for $s/B = -0.78$ (Test ML-04): (a) plan and side-view photos of the centrifuge model for $h = 3$ m, compared to (b) FE deformed mesh with superimposed plastic strains

The white dotted lines indicate the rupture trace in the free-field to allow comparison to the modified rupture pattern (black dotted lines) because of the presence of the caisson foundation.

The fault appears in the side view to follow the free-field path until it crosses the caisson sidewall. The rigid border of the caisson wall forces the rupture plane to deflect, propagating vertically along the sidewall, and emerge on its right side. A quite widespread shear failure zone appears within the lower half of the soil depth before the rupture hits the caisson—which, however, narrows progressively, localizing upon a distinct sliding plane along the top half of the caisson. Vector plots of incremental soil and caisson displacements are superimposed on the image to elucidate the fault-induced movements. The vectors confirm fault rupture diversion to the right side of the caisson, which experiences minor displacements and remains on the footwall.

A single well-defined fault scarp appears on the soil surface in the plan view [shown dotted in Fig. 7(a)]. At large horizontal distances from the foundation (see top half of the plan view photo), the fault scarp approximately follows the free-field trace, being slightly offset toward the footwall. However, upon encountering the rigid caisson body, the scarp diverts significantly—by approximately 7 m—toward the hanging wall, changing its orientation to develop along the back sidewall of the caisson and bending around the caisson's right back corner to emerge on the Perspex front face.

The numerical analysis [Fig. 7(b)] appears to predict well the fault-caisson interaction failure mechanisms described, although it shows smaller horizontal diversion of the surface scarp. The agreement between analysis and experiment for the whole range of the studied fault throws is indicated by the comparison of vertical displacement profiles measured along the centerline of the caisson (Fig. 8).

Fig. 9 presents the caisson response in terms of translational and rotational displacements measured in the centrifuge test, compared with the numerical analysis results. The analysis predicts well the translational (horizontal and vertical) displacements of the caisson for the whole range of fault throw h [Fig. 9(a)]. In terms of rotational response [Fig. 9(b)], the analysis overpredicts the amount of rotation (and translation) at low levels of throw ($h < 1.5$ m). However, analysis and experiment agree quite well at greater values of fault displacement.

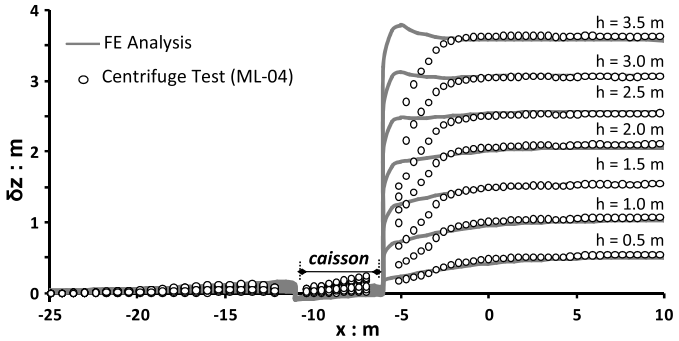

Fig. 8. Fault rupture–caisson interaction for $s/B = -0.78$ (Test ML-04): vertical displacement profiles of the model surface at different levels of fault throw and comparison with numerical results

Caisson at s/B = 0.22 with Reference to Fault (Test ML-05)

In this test, we positioned the caisson so that the free-field rupture would cross the base close to its right corner, as shown in the side-view photo in Fig. 10(a) (dotted white line). In this case, the fault interaction with the caisson results in bifurcation of the rupture and formation of two main strands, one at each side of the caisson. The two failure planes ($F1$ and $F2$) appear and evolve simultaneously.

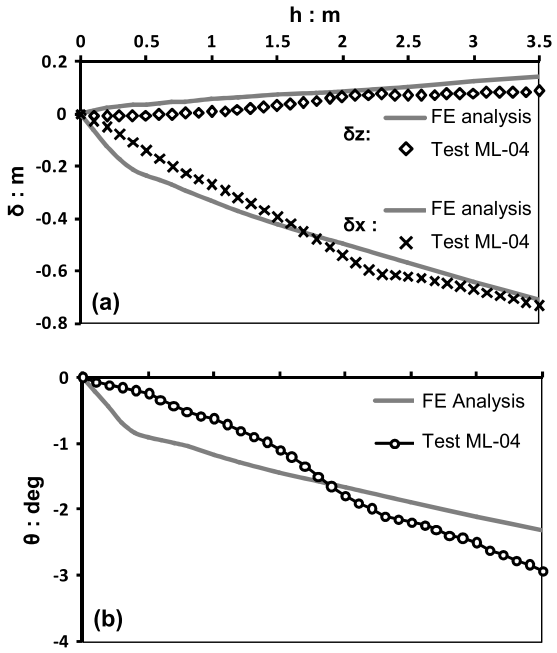

Fig. 9. Response of the caisson for $s/B = -0.78$ (Test ML-04): comparison of centrifuge with analytical results in terms of evolution with fault throw of (a) horizontal and vertical displacements, and (b) rotation

The side-view photo (bottom left) shows a relatively diffuse band of shear deformation, denoted $F1$, initiating from the bedrock dislocation and propagating with nearly vertical dip along the right sidewall of the caisson. Significant sliding occurs at the soil-foundation interface on this side, indicated by the soil heave formation near the top right corner of the caisson. The heave height (relative displacement between the caisson right corner and the soil surface) reaches nearly 2.5 m for $h = 3.5$ m, suggesting that $F1$ is the plane where most of the fault deformation occurs. Nevertheless, a secondary localization appears ($F2$), which propagates from the bedrock dislocation toward the left (footwall) side of the caisson. Intersecting with the base left corner of the caisson, $F2$ propagates with an approximately constant dip angle of about 30° (half of the bedrock dip angle) past the caisson. Because of the relatively shallow dip angle, $F2$ does not reach the surface for fault throw $h < 3$ m. However, a scarp forms at the soil surface at the position that $F2$ outcrops. This is visible in the side-view photo (bottom left) for $h = 3.5$ m.

The incremental displacement vectors in Fig. 10(a) show that the caisson translates with the hanging wall, being evidently more distressed than in the case previously studied. (Recall that in that test, the caisson remained on the footwall practically nondisplaced.) Hence, the caisson experiences significant translational and rotational displacements.

In the plan view image in Fig. 10(a) (top left), the surface fault rupture differs significantly from the free-field pattern. It is evidently affected by the caisson even at a distance of more than $3B$ from the caisson centerline in the transverse direction [upward in Fig. 10(a)]. At this distance, two surface scarps are visible, propagating on the surface parallel to the free-field trace. The surface fault deformation zone expands in width as the rupture moves closer to the caisson, and the two rupture planes ($F1$ and $F2$) diverge, one toward the hanging wall and the other toward the footwall. Furthermore, the surface scarp of $F2$ forms secondary strands, implying progressive shift of the fault outcrop toward the footwall.

Fig. 10(b) illustrates the computed failure mechanisms in terms of plastic strain contours superimposed on the deformed FE mesh. The analysis captures well the previously described interaction

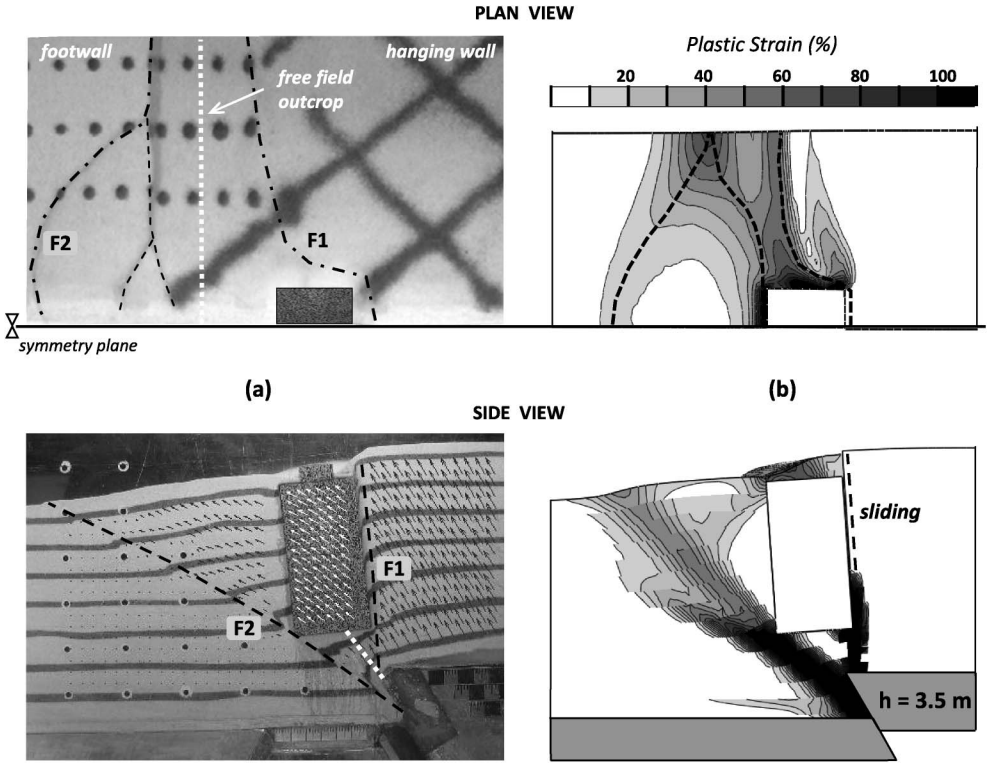

Fig. 10. Fault rupture–caisson interaction mechanisms for $s/B = 0.22$ (Test ML-05): (a) plan and side-view photos of the centrifuge model for $h = 3.5$ m, compared to (b) FE deformed mesh with superimposed plastic strains

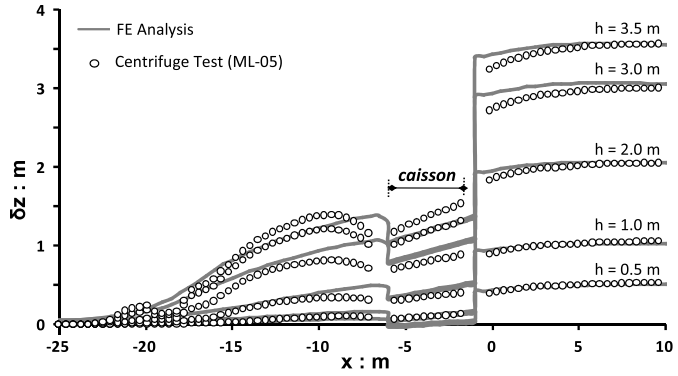

Fig. 11. Fault rupture–caisson interaction for $s/B = 0.22$ (Test ML-05): vertical displacement profiles of the model surface at different levels of fault throw and comparison with numerical results

mechanisms and is in satisfactory agreement with the experiment. The effectiveness of the numerical method is also demonstrated by the satisfactory comparison of displacement profiles at the model surface (Fig. 11). Regarding the caisson response, Fig. 12 shows that the analysis underestimates slightly the caisson uplift (δz) at great magnitudes of fault throw, yet it predicts quite accurately the horizontal displacement and rotation for the whole range of examined fault throws.

Caisson at s/B = 0.62 with Reference to Fault (Test ML-03)

In this final centrifuge test, we placed the caisson so that the free-field rupture would interact with its left base corner (toward the footwall). The deformed centrifuge model photos [Fig. 13(a)] suggest that the fault rupture splits again in two components ($F1$ and $F2$). Compared to the previous test, $F1$ is now the main localization along which most of the faulting deformation accumulates. This localization appears to deflect toward the footwall (to the left), just

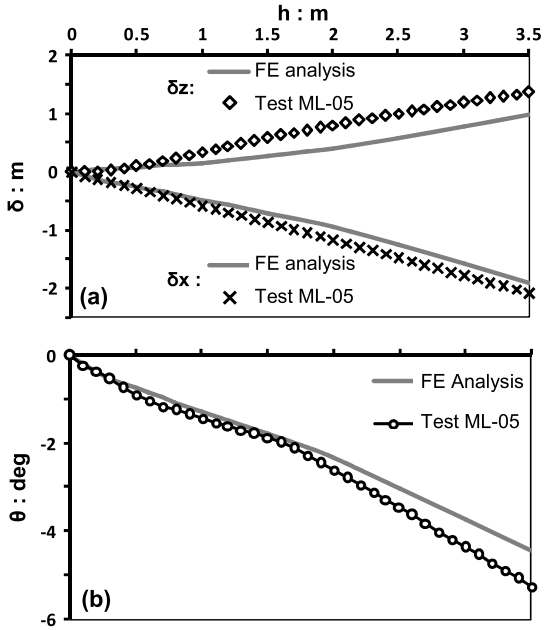

Fig. 12. Response of the caisson for $s/B = 0.22$ (Test ML-05): comparison of centrifuge with analytical results in terms of evolution with fault throw of (a) horizontal and vertical displacements, and (b) rotation

intersecting the left base corner of the caisson. $F2$ initiates from the bedrock dislocation and intersects with the right base corner, causing sliding deformation along the sidewall of the caisson. Because the right edge of the caisson is to the right of the bedrock fault, $F2$ is forced to propagate antithetically, i.e., with a dip angle that contradicts the direction of the predominant mode of faulting.

As for the previous cases, the plan view [top left in Fig. 13(a)] demonstrates the wide influence zone of the caisson at the surface. The caisson proves capable of modifying the fault rupture scarp within a radius exceeding 16 m (nearly $3B$). Again, the two fault scarps tend to diverge when approaching the caisson. More specifically, $F1$ bends toward the footwall (observe the formation of a secondary scarp, as in the previous case), and $F2$ deflects toward the hanging wall, abruptly changing in strike, and then twists around the caisson to emerge on its right (hanging wall) side on the plane of symmetry.

Fig. 13(b) demonstrates qualitative agreement between the FE prediction and experimental observations regarding the mechanisms of fault rupture–caisson interaction. The numerical analysis captures the diversion of the fault to the left (toward the footwall) of the caisson and the sliding plane formation along its right sidewall. This is also evident in the plots of vertical (δz) surface displacement profiles (Fig. 14), which indicate good agreement between analysis and experiment regarding the position of the fault emergence for all levels of fault offset. Equally satisfactory is the comparison of δz to the right (hanging wall) side of the caisson. The analysis underestimates the amount of sliding deformation occurring along the right (hanging wall) side of the caisson. As a result, the caisson uplift is overestimated, which in turn results in an exaggerated prediction of the height of soil heave that forms at the left of the caisson for the largest fault throws. This discrepancy becomes evident for $h > 2$ m.

Fig. 15 confirms this discrepancy between analysis and experiment regarding the caisson uplift δz for fault throws greater than 2 m. However, the comparison is quite satisfactory in terms of horizontal (δx) and rotational (θ) displacements, even for $h > 2.0$ m. Thus, we can claim that the overall system performance is well predicted.

Numerical Parametric Study on Effect of Exact Caisson Position

The foregoing analysis highlighted the determinative role of the caisson position and suggested that the main features of fault rupture–caisson interaction can be captured by the numerical analysis method employed herein. For this reason, we considered it worthwhile to investigate further the effect of the exact caisson position relative to the fault rupture using a numerical parametric study. The key results and conclusions of this study are discussed in this section.

Fig. 16 presents a set of graphs showing the displacement response (translational displacement, δz and δx; and rotation, θ) of the caisson for four different amplitudes of fault throw (h), as calculated from a series of 22 FE analyses, each with the foundation located in a different position (s) in relation to the fault. To allow comparison, centrifuge test results are also indicated using circular points for the same fault throws. The numbers in square brackets [in Fig. 16(c)] correspond to the adjacent FE deformed meshes, which indicate the different rupture-caisson interaction mechanisms taking place for different caisson positions. We identify the following modes of response:

For $-1 < s/B < -0.6$, when the fault rupture interacts with the upper half of the caisson right sidewall (1), the rupture is diverted

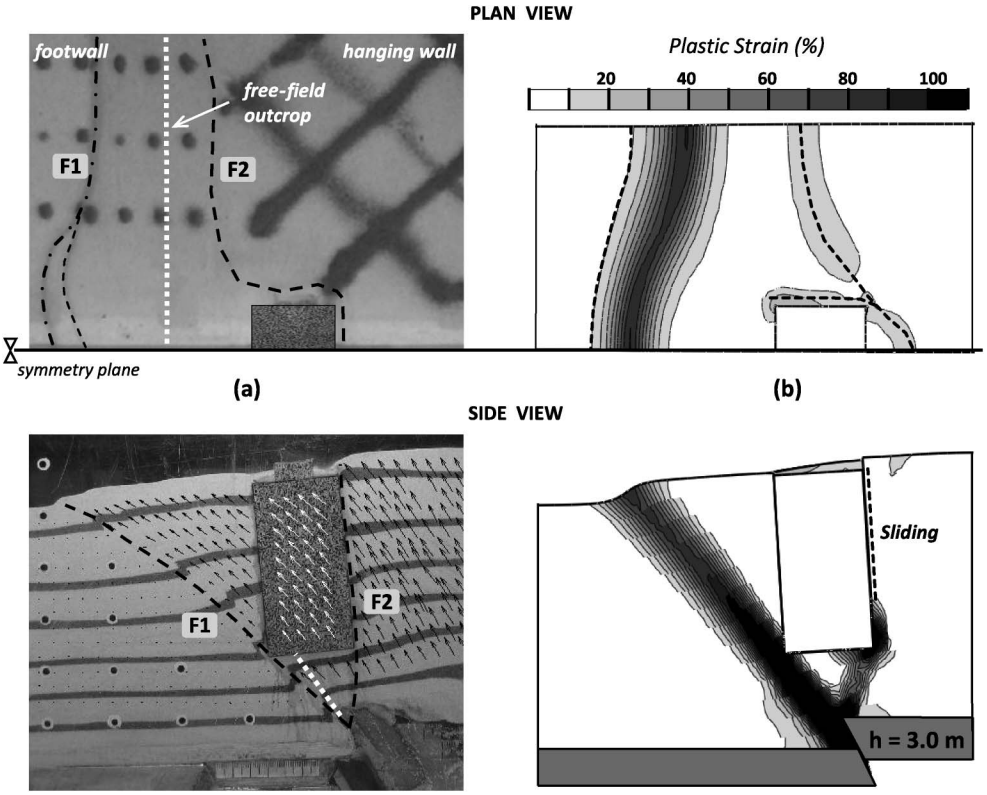

Fig. 13. Fault rupture–caisson interaction mechanisms for $s/B = 0.62$ (Test ML-03): (a) plan and side-view photos of the centrifuge model for 3 m of fault throw, compared to (b) FE deformed mesh with superimposed plastic strains

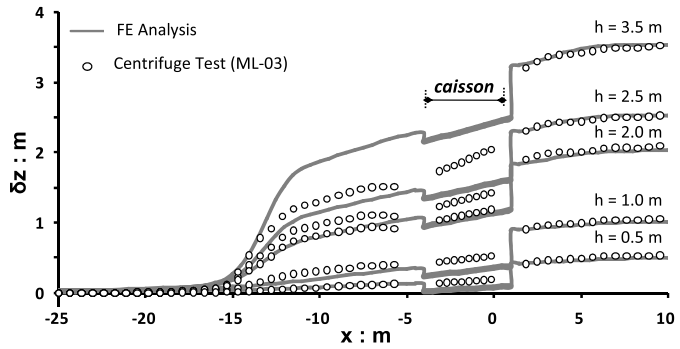

Fig. 14. Fault rupture–caisson interaction for $s/B = 0.62$ (Test ML-03): vertical displacement profiles of the model surface at different levels of fault throw and comparison with numerical results

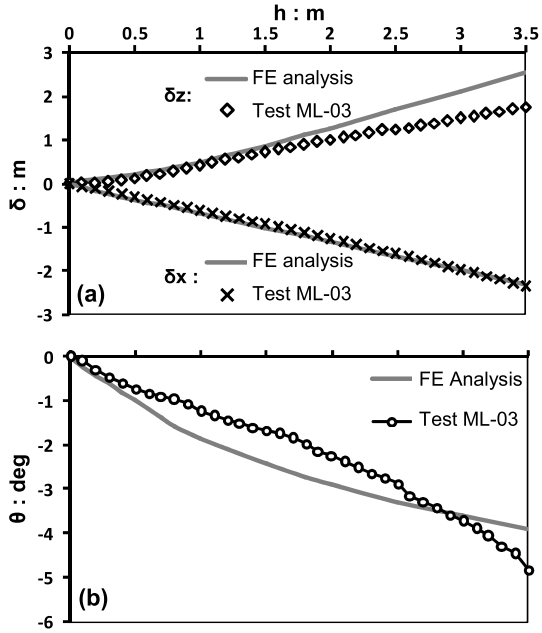

Fig. 15. Response of the caisson for $s/B = 0.62$ (Test ML-03): comparison of centrifuge with analytical results in terms of evolution with fault throw of (a) horizontal and vertical displacements, and (b) rotation

toward the hanging wall and the caisson remains on the footwall. As a result, it experiences limited distress, being subjected to relatively small rotational and horizontal displacement, and practically zero uplift. This zone of s/B is clearly the most favorable; we discussed it in greater detail in the representative case of Test ML-04.

Increasing s/B for $-0.6 \leq s/B < -0.1$ results in an abrupt increase of caisson rotation θ and horizontal displacement δx and a less striking yet significant rise of caisson uplift δz. As for the previous case, the fault interacts only with the right sidewall of the caisson, being diverted toward the hanging wall (to the right), and a significant amount of sliding takes place at the interface. The shearing stresses developing along a greater area of the sidewall lead to significant caisson rotation and consequently to amplified horizontal movement of the reference point. When the fault interacts with the caisson right base corner [mesh (2)], the rupture "grazes" the caisson's right sidewall along its entire length. For $h > 1$ m, this is the worst position for the foundation in terms of rotation θ.

Moving the caisson farther toward the hanging wall (for $-0.1 \leq s/B < 0.3$) causes the fault rupture to bifurcate and a

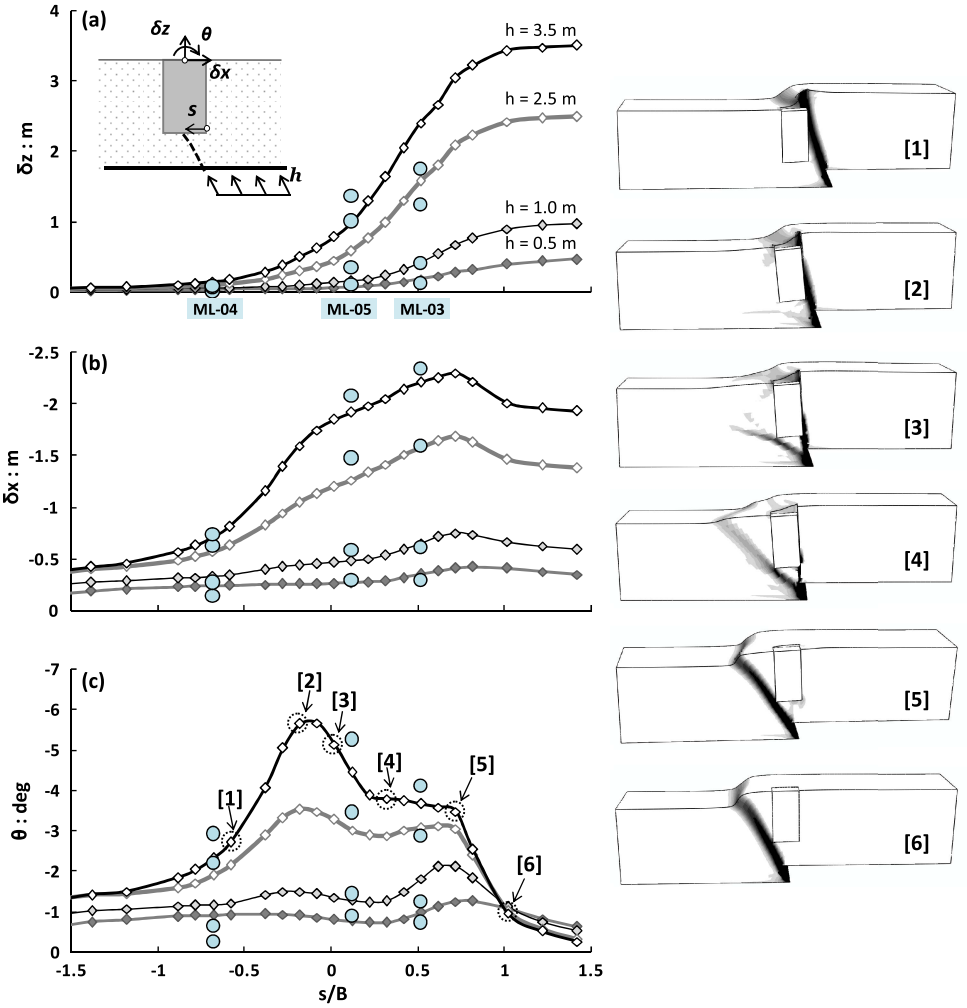

Fig. 16. The effect of the exact caisson location (s) on the mechanisms of fault rupture–caisson interaction and the consequent response of the caisson: (a) vertical displacements, (b) horizontal displacements, and (c) rotation for different levels of fault throw; numbers in square brackets refer to labeled FE deformed models; circular points in the graphs indicate corresponding experimental results from the three centrifuge tests

secondary fault plane to form, propagating toward the left (footwall) caisson side (3). The interaction of this secondary fault plane with the caisson left base corner acts as a balancing force that counteracts the anticlockwise rotating effect of the main rupture (on the right side). Hence, the rotational response is limited compared to that of the previous case [see (2)]. However, this is not true for the translational displacements, which increase as the caisson stands now on the moving block (the hanging wall).

The left side localization becomes the predominant deformation mechanism for $s/B = 0.32$ [at (4)]. Interestingly, for $0.3 \leq s/B < 0.7$, the rotation θ of the caisson appears to be insensitive to its exact position, at least for large values of fault throw [see the plateau in Fig. 16(c) from (4) to (5)]. In contrast, for small throws, $h < 1.0$ m, the fault has not propagated adequately toward the surface and the response is controlled by the quasi-elastic deformation of the hanging wall. This explains the peak in θ for low fault bedrock offsets when $s/B \approx 0.75$, where the caisson stands entirely on the hanging wall, thus following its quasi-elastic deformation.

For s/B greater than 0.7, the fault rupture diverts toward the caisson footwall side, intersecting at its left base corner [(5), (6)]. This leads to an abrupt decrease of θ, which is virtually eliminated for $s/B > 1.0$ (i.e., when practically no interaction exists between the fault rupture and the caisson). The caisson experiences pure translational displacement, moving along with the hanging wall.

Conclusions

We have presented a combined experimental and numerical study of the interaction among a reverse fault rupture, the soil, and an embedded rigid caisson foundation. Although the study unavoidably is focused on a specific geometry and soil profile, we believe that the observed mechanisms and the resulting caisson behavior are at least qualitatively of more general validity. In a similar problem of a reverse fault interacting with a caisson foundation, one would anticipate that the fault-caisson interaction mechanism would follow one of the previously identified modes of response (Fig. 16), mainly depending on the relative foundation position. However, although the caisson would in any case respond through rigid-body translation and rotation, the magnitude of its displacement is sensitive to the characteristics of the problem (geometry, soil parameters, foundation surcharge load), and presumably the presented quantitative results refer to the specific case examined herein.

We summarize the key conclusions of this study as follows:

- We studied reverse fault rupture propagation in the free field; both numerical and experimental results regarding the propagation and the position of the failure surface were in reasonable agreement with field observations and former research studies.
- We investigated experimentally the mechanism of fault rupture–caisson interaction for three different cases of foundation

position relative to the free-field fault. The rigid caisson acted as a kinematic constraint, causing complete diversion of the fault rupture and forcing it to develop outside the foundation margins. We believe that this is a significant advantage of caissons compared with less flexible foundation types (e.g., shallow foundations), and the results supply encouraging evidence for the recently raised idea that such rigid foundation types can be used in designing fault-resistant structures (Gazetas et al. 2008).

- However, the mechanism and direction of the fault diversion and its effect on the performance of the caisson varied significantly depending on its position relative to the free-field rupture. When the free-field rupture crossed the right sidewall of the caisson (Test ML-04), the fault deviated to the right (toward the hanging wall), leaving the caisson practically unscathed on the stationary footwall side. Despite remaining on the nondisplaced side of the ground (footwall), the caisson underwent significant rotation as the rupture grazed its hanging wall side, generating significant frictional stresses at the soil-caisson interface. In particular, this mechanism of fault-caisson interaction results in the maximum rotation that the caisson may undergo for greater than 2 m of fault offset [Fig. 16(c)]. This result is in qualitative agreement with the case history of the Chi-chi electricity pylon (Fig. 2), which is believed to have been subjected to a very similar fault-caisson interaction mechanism.
- The fault-caisson interaction mechanism was less distinct when the free-field rupture crossed the right side of the caisson base (Test ML-05). We observed bifurcation of fault rupture, and the fault deformation split in two strands, one along each foundation side. Soil failure around the foundation resulted in significantly larger displacements, as well as particularly large caisson rotations compared to the previous case (Test ML-04).
- Moving the free-field rupture–caisson intersection point farther left (Test ML-03) resulted in diversion of the fault rupture toward the footwall and secondary sliding plane formation along the caisson wall on its hanging wall side. The caisson underwent significant rotation and the largest translational displacement of all tests: In this case, it translated *with* the hanging wall.
- We validated the numerical method by successfully comparing it with centrifuge test results, revealing its effectiveness in capturing qualitatively and quantitatively the mechanisms of fault rupture–caisson interaction. From this, we are confident that the same method can be used to study similar problems or that it may be used as a design tool.
- The caisson's zone of influence was quite widespread, and at times it modified the surface fault rupture within a radius that exceeded three times its width. In other words, a wider (more than three times the foundation breadth in width) physical and numerical model should be used to eliminate completely the spurious effects of lateral boundaries. These effects were explored numerically by varying the distance of the caisson to the boundary from 2*B* to 5*B* (in which *B* is the breadth of the caisson). We concluded that to have no boundary effects at all, the distance should be equal to 5*B*, which is qualitatively equivalent to the zone of influence of a pile (for example, Reese and Van Impe 2001). However, Fig. 17 shows, even for the minimum distance of 2*B*, the response of the caisson is practically identical to that of 5*B*: the discrepancies between the two extreme cases are less than 2%. Hence, one may consider the experimental and numerical results presented herein to be practically unaffected by the lateral boundary.
- We further investigated parametrically the effect of the exact caisson position in a numerical study that revealed several interaction mechanisms and highlighted the sensitivity of response to this parameter. Given that the position of the fault outcrop in the event of an earthquake cannot be estimated with sufficient

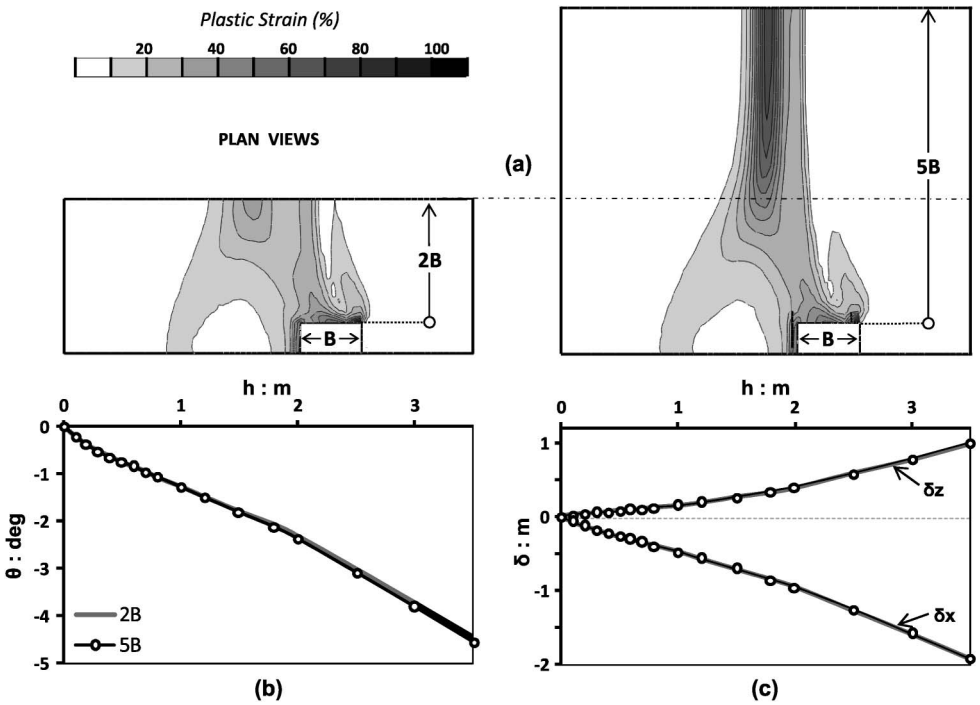

Fig. 17. Numerical investigation of the effect of the lateral boundary in the transverse direction (*y*-axis); comparison of two extreme cases, in which the lateral boundary is set at horizontal distance 2*B* (minimum) and 5*B* (maximum) in terms of (a) plan view of the computed surface fault rupture, as illustrated through the deformed FE meshes with superimposed plastic strain contours, for $h = 3.5$ m; (b) evolution of caisson rotation θ; and (c) translational displacements relating to the applied fault throw h

accuracy, even in the case of known existing faults, one can only implement the fault-resistant design of structures with regard to response envelopes of displacement and rotation, such as those shown in Fig. 16. Having proved to be adequately valid and relatively time efficient, the presented numerical method can be used to construct such response envelopes, and it can be implemented in the design of structures on caisson foundations against fault loading.

Acknowledgments

National Technical University of Athens (NTUA) authors would like to acknowledge financial support from the European Union Seventh Framework Programme (FP7), funded through the European Research Council's Program "Ideas," Support for Frontier Research Advanced Grant, under Contract No. ERC-2008-AdG 228254-DARE.

References

Ahmed, W., and Bransby, M. F. (2009). "The interaction of shallow foundations with reverse faults." *J. Geotech. Geoenviron. Eng.*, 135(7), 914–924.

Anastasopoulos, I., Antonakos, G., and Gazetas, G. (2010). "Slab foundation subjected to thrust faulting in dry sand: Parametric analysis and simplified design method." *Soil Dyn. Earthquake Eng.*, 30, 912–924.

Anastasopoulos, I., and Gazetas, G. (2007a). "Foundation-structure systems over a rupturing normal fault: Part I. Observations after the Kocaeli 1999 earthquake." *Bull. Earthquake Eng.*, 5(3), 253–275.

Anastasopoulos, I., and Gazetas, G. (2007b). "Behaviour of structure-foundation systems over a rupturing normal fault: Part II. Analysis of the Kocaeli case histories." *Bull. Earthquake Eng.*, 5(3), 277–301.

Anastasopoulos, I., Gazetas, G., Bransby, M. F., Davies, M. C. R., and El Nahas, A. (2007c). "Fault rupture propagation through sand: Finite element analysis and validation through centrifuge experiments." *J. Geotech. Geoenviron. Eng.*, 133(8), 943–958.

Anastasopoulos, I., Gazetas, G., Bransby, M. F., Davies, M. C. R., and El Nahas, A. (2009). "Normal fault rupture interaction with strip foundations." *J. Geotech. Geoenviron. Eng.*, 135(3), 359–370.

Anastasopoulos, I., Gazetas, G., Drosos, V., Georgarakos, T., and Kourkoulis, R. (2008). "Design of bridges against large tectonic deformation." *Earthquake Eng. Eng. Vib.*, 7, 345–368.

Angelier, J., Lee, J.-C., Hu, J.-C., and Chu, H.-T. (2003). "Three-dimensional deformation along the rupture trace of the September 21st, 1999, Taiwan earthquake: A case study in the Kuangfu school." *J. Struct. Geol.*, 25, 351–370.

Bolton, M. D. (1986). "The strength and dilatancy of sands." *Géotechnique*, 36(1), 65–78.

Bransby, M. F., Davies, M. C. R., El Nahas, A., and Nagaoka, S. (2008a). "Centrifuge modelling of normal fault-foundation interaction." *Bull. Earthquake Eng.*, 6(4), 585–605.

Bransby, M. F., Davies, M. C. R., El Nahas, A., and Nagaoka, S. (2008b). "Centrifuge modelling of reverse fault-foundation interaction." *Bull. Earthquake Eng.*, 6(4), 607–628.

Bray, J. D., Seed, R. B., Cluff, L. S., and Seed, H. B. (1994a). "Analysis of earthquake fault rupture propagation through cohesive soil." *J. Geotech. Eng.*, 120(3), 562–580.

Bray, J. D., Seed, R. B., Cluff, L. S., and Seed, H. B. (1994b). "Earthquake fault rupture propagation through soil." *J. Geotech. Eng.*, 120(3), 543–561.

Chang, K.-C., Chang, D.-W., Tsai, M.-H., and Sung, Y.-C. (2000). "Seismic performance of highway bridges." *Earthquake Eng. Eng. Seismol.*, 2(1), 55–77.

Cole, D. A., Jr., and Lade, P. V. (1984). "Influence zones in alluvium over dip-slip faults." *J. Geotech. Eng.*, 110(5), 599–615.

Dong, J. J., Wang, C. D., Lee, C. T., Liao, J. J., and Pan, Y. W. (2004). "The influence of surface ruptures on building damage in the 1999 Chi-chi earthquake: A case study in Fengyuan City." *Eng. Geol.*, 71, 157–179.

El Nahas, A., Bransby, M. F., and Davies, M. C. R. (2006). "Centrifuge modelling of the interaction between normal fault rupture and rigid, strong raft foundations." *Proc., Int. Conf. on Physical Modelling in Geotechnics*, Int. Society of Soil Mechanics and Geotechnical Engineering, Hong Kong Univ. of Science and Technology, Hong Kong, 337–342.

Faccioli, E., Anastasopoulos, I., Callerio, A., and Gazetas, G. (2008). "Case histories of fault-foundation interaction." *Bull. Earthquake Eng.*, 6, 557–583.

Gaudin, C. (2002). "Modélisation physique et numérique des écrans de soutènement: Application à l'étude de l'effet d'une surcharge sur le sol soutenu." Ph.D. thesis, Univ. de Nantes, Nantes, France.

Gazetas, G., Anastasopoulos, I., and Apostolou, M. (2007). "Shallow and deep foundations under fault rupture or strong seismic shaking." Chapter 9, *Geotechnical earthquake engineering*, Springer, 185–217.

Gazetas, G., Pecker, A., Faccioli, E., Paolucci, R., and Anastasopoulos, I. (2008). "Design recommendations for fault–foundation interaction." *Bull. Earthquake Eng.*, 6, 677–687.

GeoPIV-8. (2007). [Computer software]. Cambridge, U.K., Cambridge Univ. Engineering Department.

Jia, D., et al. (2010). "Structural model of 2008 M_W 7.9 Wenchuan earthquake in the rejuvenated Longmen Shan thrust belt, China." *Tectonophysics*, 491(1–4), 174–184.

Kawashima, K. (2001). "Damage of bridges resulting from fault rupture in the 1999 Kocaeli and Düzce, Turkey earthquakes and the 1999 Chi-chi, Taiwan earthquake." *Workshop on seismic fault-induced failures: Possible remedies for damage to urban facilities*, University of Tokyo, Tokyo, 171–190.

Kelson, K. I., et al. (2001a). "Fault-related surface deformation." *Earthquake Spectra*, 17 (Supplement A: Chi-chi, Taiwan, earthquake of September 21, 1999, reconnaissance report), 19–36.

Kelson, K. I., Kang, K.-H., Page, W. D., Lee, C.-T., and Cluff, L. S. (2001b). "Representative styles of deformation along the Chelungpu fault from the 1999 Chi-chi (Taiwan) earthquake: Geomorphic characteristics and response of man-made structures." *Bull. Seismol. Soc. Am.*, 91(5), 930–952.

Lin, A., Ren, Z., Jia, D., and Wu, X. (2009). "Co-seismic thrusting rupture and slip distribution produced by the 2008 M_W 7.9 Wenchuan earthquake, China." *Tectonophysics*, 471(3–4), 203–215.

Lin, A., and Ren, Z. (2009). *The great Wenchuan earthquake of 2008: A photographic atlas of surface rupture and related disaster*, Springer, Berlin.

Loukidis, D., Bouckovalas, G., and Papadimitriou, A. G. (2009). "Analysis of fault rupture propagation through uniform soil cover." *Soil Dyn. Earthquake Eng.*, 29(11–12), 1389–1404.

Paolucci, R., and Yilmaz, M. T. (2008). "Simplified theoretical approaches to earthquake fault rupture–shallow foundation interaction." *Bull. Earthquake Eng.*, 6(4), 629–644.

Reese, L. C., and Van Impe, W. F. (2001). *Single piles and pile groups under lateral loading*, A. A. Balkema, Rotterdam/Brookfield, Netherlands.

Roth, W. H., Sweet, J., and Goodman, R. E. (1982). "Numerical and physical modelling of flexural slip phenomena and potential for fault movement." *Rock Mechanics Supplementum*, Supplement 12, 27–46.

Schofield, A. N. (1980). "Cambridge University geotechnical centrifuge operations." *Géotechnique*, 30(3), 227–268.

Sherard, J. L., Cluff, L. S., and Allen, C. R. (1974). "Potentially active faults in dam foundations." *Géotechnique*, 24(3), 367–428.

White, D. J., Take, W. A., and Bolton, M. D. (2003). "Soil deformation measurement using particle image velocimetry (PIV) and photogrammetry." *Géotechnique*, 53(7), 619–631.

Xu, X., et al. (2009). "Coseismic reverse- and oblique-slip surface faulting generated by the 2008 M_W 7.9 Wenchuan earthquake, China." *Geology*, 37(6), 515–518.

Yilmaz, M. T., and Paolucci, R. (2007). "Earthquake fault rupture–shallow foundation interaction in undrained soils." *Earthquake Eng. Struct. Dyn.*, 36, 101–118.